Bollettino di Geofisica Teorica ed Applicata Vol. 56, n. 1, pp. 19-30; March 2015
DOI 10.4430/bgta0134

Detecting, modelling and reserve estimating of manganese ore bodies via microgravity data

V.E. Ardestani

Institute of Geophysics, University and Center of Excellency in Survey Engineering and Disaster Management, Tehran, Iran

(Received: May 19, 2014 2014; accepted: December 15, 2014)

ABSTRACT A microgravity survey was carried out for detecting, modelling and estimating the reserve of a manganese ore body in an area with a hilly topography close to Zereshloo village in the NW of Iran. An outcrop of ore body exists in the area and the data were collected in a network around the outcrop. The data was reduced and processed by standard techniques and software. A 3D inversion package was applied for modelling and estimating the reserve of the ore body. To confirm the 3D inversion results, several bore-holes were drilled in the area. The 3D inversion results of depth and density contrast of the main anomaly were confirmed by the bore-holes.

Key words: detection, 3D inversion, reserve estimation, microgravity data, Zereshloo site.

1. Introduction

Microgravity has been applied by several researchers in the fields of environmental and engineering geophysics. The most frequent issues of these fields are cavity or Karst detection, landslides and geotechnical surveys such as detecting and modeling the low-density zones.

Several pioneer papers are published in this regard such as Arzi (1975), Fajklewicz (1976), Butler (1984) and Ardestani (2008, 2010).

Microgravity is also used for mineral explorations and is not used particularly for reserve estimations which are the main information for the most mining exploration companies and individuals.

2. Location and geology of the survey area

The survey area was located between Mianeh and Tabriz cities close to Zereshloo village with a hilly topography in the NW of Iran.

The survey area was located in an area named Sanadaj Sirjan in Zagros Mountain (Noorizadeh, 2010). The main geological units in the area were altered andesite with hematite and bazaltic tuff with olivine and pyroxene. The ore body was mainly pyrolusite mixed with manganite, psilomelan and hematite in some places. There was a main outcrop of ore body in the northern part of the survey area which is pointed in Fig. 1. The grade of the manganese

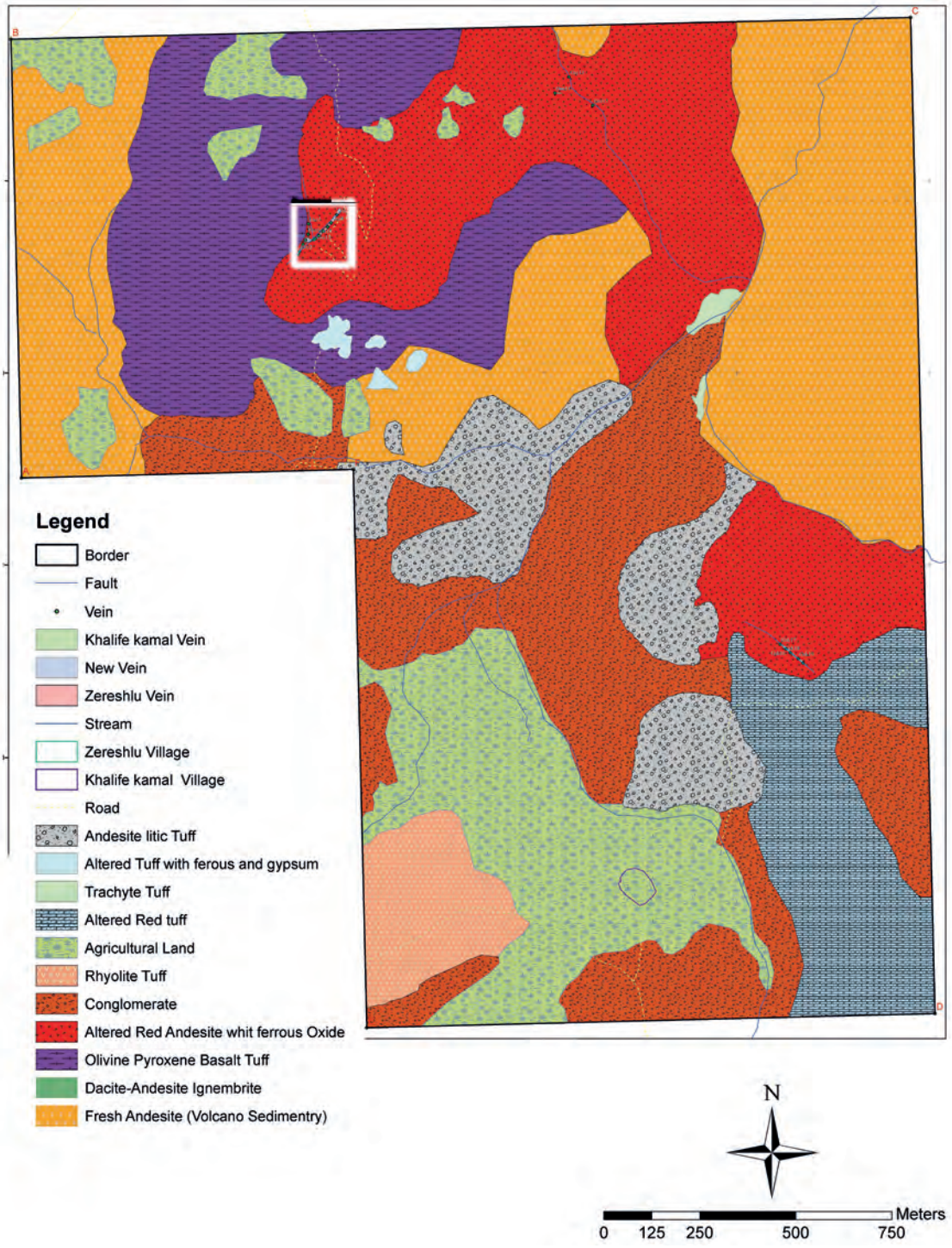

Fig. 1 - The survey area and geological map.

was between 18 and 60% in the samples of the ore bodies obtained from the survey area (Noorizadeh, 2010).

3. Microgravity measurements

A ScintrexCG3 gravimeter with a sensitivity of 5 μGal was used for microgravity observations in the survey area. The station altitude was measured with a total station model Leica Tc407 with an accuracy of 5-10 mm in horizontal and vertical coordinates. The gravity and altitude measurements were undertaken by the gravity branch of the Institute of Geophysics, Tehran University in March of 2010 and under the supervision of the author. The gravity network consisted of 1000 measurement points in a grid of 5 to 10 m grid spacings between measurement stations.

4. Gravity reductions

The raw gravity measurements were tied to a base point in the lowest part of the topography. The long-term drift of the gravimeter was removed by using the cycling mode of the gravimeter over several days at the office in Tehran. For removing the short-term drift, the gravity acceleration was measured on the base point several times during the work day. The maximum short-term drift during a work day was 20 μGal. The data was then corrected for effects caused by variations in latitude, elevation, and topography. The equation for the latitude correction is (Telford *et al.*, 1981):

$$g_l = 0.000812132(\sin 2l)y_s \tag{1}$$

where g_l is the latitude correction, l is latitude of station and y_s is the station distance north of the grid origin in metre. It is worth to mention that, due to the local base station as the reference point for relative heights and gravity, Eq. (1) is applied for latitude correction instead of full correction standard form.

Free-air and Bouguer corrections were computed through standard equations and considering the relative heights. The average density required for the Bouguer correction was defined from previous information (Noorizadeh, 2010) as 2500 kg/m^3.

The terrain correction is usually the most sensitive stage in gravity reductions. This correction was calculated using a combination of the methods described by Kane (1962) and Nagy (1966). To calculate the local corrections, the local Digital Terrain Model (DTM) was "sampled" to a grid mesh centered on the station to be calculated. The grid sampled spacings in the local and regional grids were 2 and 5 m, respectively. The correction was calculated based on near zone and far zone contributions applying the local and regional grids. In the near zone (0 to 1 cells from the station), the algorithm sums the effects of four sloping triangular sections, which describe a surface between the gravity station and the elevation at each diagonal corner in Eq. (2) (Kane, 1962):

$$g_i = G\rho\Phi\left(R - \sqrt{R^2 + H^2} + \frac{H^2}{\sqrt{R^2 + H^2}}\right) \tag{2}$$

where g_i is the gravity effect, G is the gravitational constant, ρ is the density, R is the length of

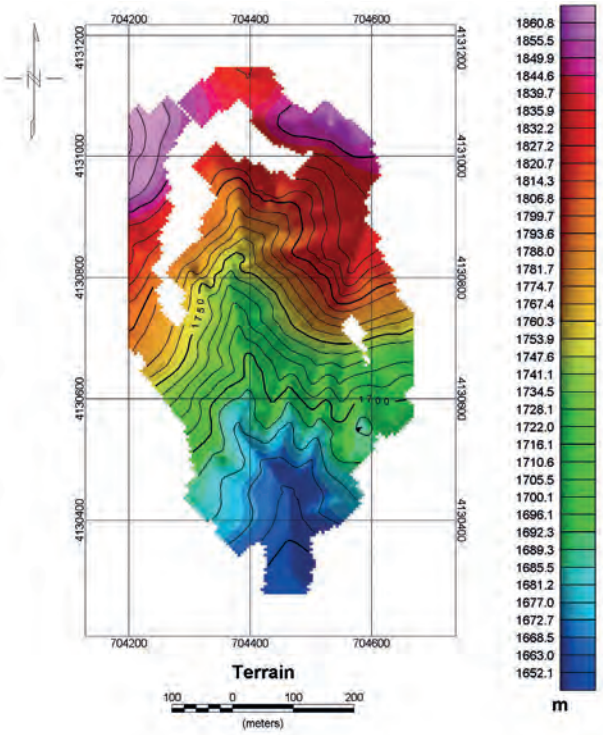

Fig. 2a - Topographical heights (m).

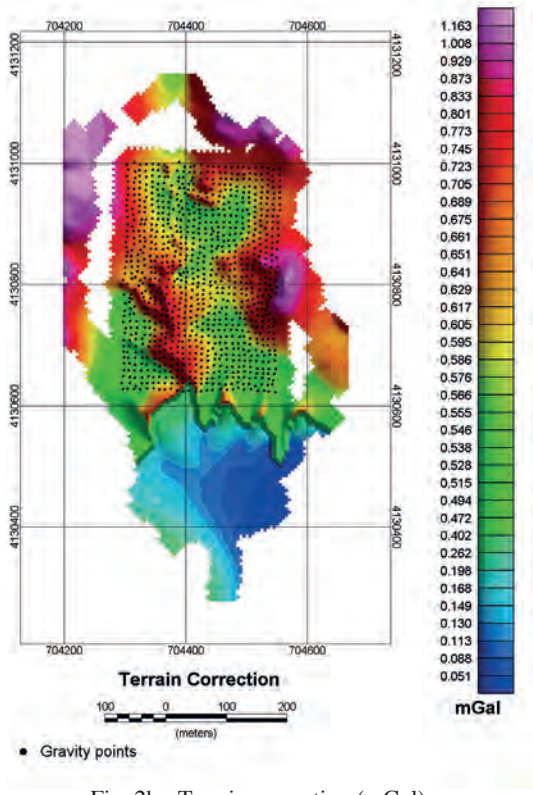

Fig. 2b - Terrain correction (mGal).

the triangle, H is the elevation at the diagonal corner, and Φ is the horizontal angle between the station and the horizontal diagonal corners.

In the far zone (1 to end cells from the station), the terrain effect was calculated for each point using the flat topped square prism approach of Nagy (1966):

$$g = -G\rho \left| \begin{matrix} z2 \\ z1 \end{matrix} \right| \left| \begin{matrix} y2 \\ y1 \end{matrix} \right| \left| \begin{matrix} x2 \\ x1 \end{matrix} \right| x \ln(y+R) + y \ln(x+R) + z tg^{-1}\left(\frac{z.R}{x.y}\right) \left| \right| \left| \right| \quad (3)$$

where g is the gravity effect of the prism, G is the gravitational constant, ρ the density and $x1$, $y1$, $z1$ and $x2$, $y2$, $z2$ are the Cartesian coordinates of the left lowermost and right uppermost corners of the prism in a right angle coordinate system, respectively and:

$$R = \sqrt{x^2 + y^2 + z^2} \quad . \quad (4)$$

As the height of the gravity points were measured accurately, we included these points in the DTM to make it as dense as possible. The adjacent topography of the gravity network up to 100 and in some directions 200 m were also surveyed (Fig. 2a). Terrain corrections using the presented formulae in near and far zone contributions were computed and the results are shown in Fig. 2b. Due to a shortage of terrain data, there are some gaps in topographical corrections (white color in Fig. 2b).

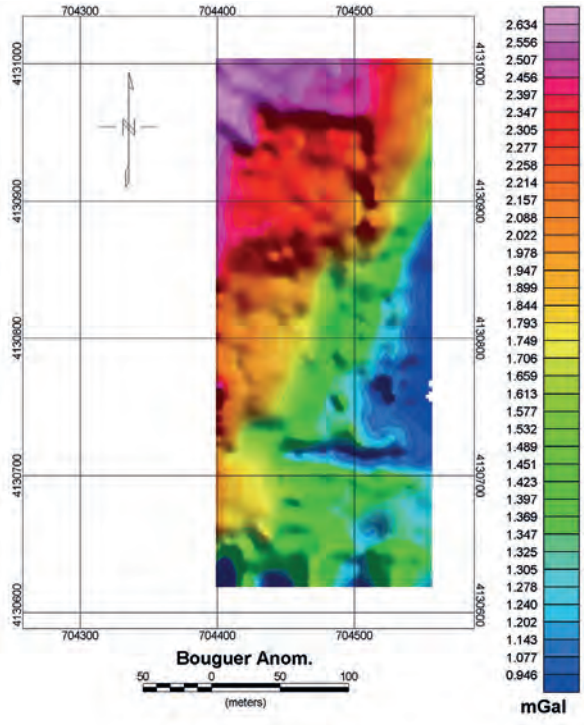

Fig. 3 - Bouguer anomalies (mGal).

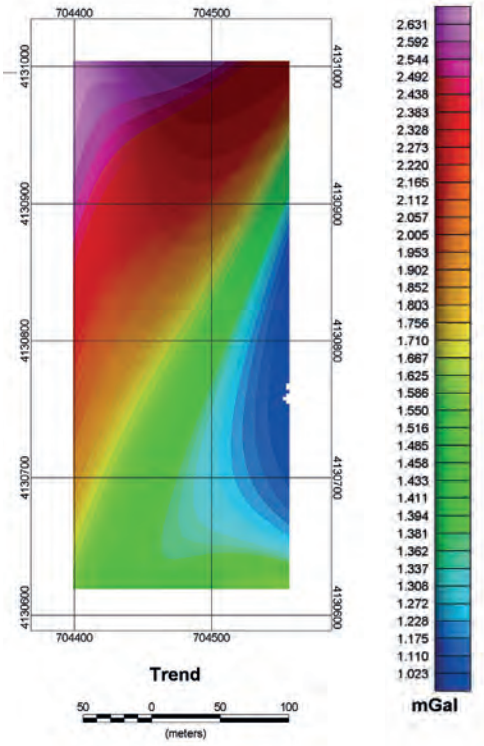

Fig. 4 - Trend anomalies (mGal).

Applying these corrections, the Bouguer gravity anomalies were computed and the results are shown in Fig. 3. The statistical values for topographical corrections and Bouguer anomalies in the measured points are reflected in Table 1:

Table 1 - Statistical values for topographical correction and Bouguer anomalies.

Values	Minimum (mGal)	Maximum (mGal)	Average (mGal)	Standard Deviation (mGal)
Topographical corrections	0.015	0.73	0.25	0.12
Bouguer anomalies	0.070	4.19	1.80	0.53

The values in Table 1 confirm the sufficient accuracy of the topographical corrections in the survey area.

For high-lighting the local anomalies with removing the trend effect, the residual anomalies are computed by using the polynomial fitting method. This removed trend effect is shown in Fig. 4.

One of the equations for constructing these polynomials is the following formula:

$$g(x,y) = \sum_{q=0}^{t} \sum_{p=0}^{s} V_{pq} x_i^p y_i^q \qquad (5)$$

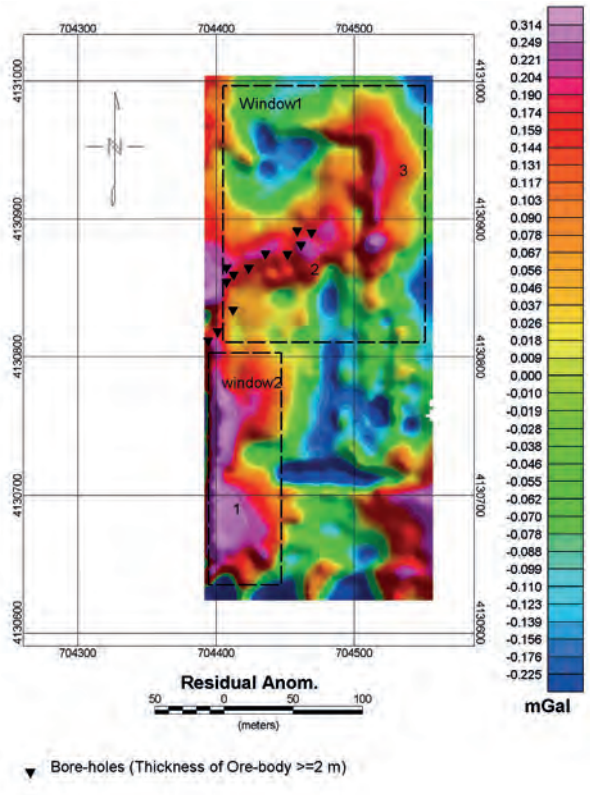

Fig. 5 - Residual anomalies and the selected windows for 3D modeling and the bore-holes (mGal).

where q is the degree and V represent the indexes of the polynomial which have to be computed through least-square method and x and y are the coordinates of the gravity points. g is the regional gravity anomaly that with subtracting it from Bouguer anomalies, the residual anomalies will be computed in each point Fig. 5.

The positive anomalies which can be caused by ore bodies were numbered from 1 to 3. The main positive anomaly was Number 2 and the outcrop belonged to the western part of this anomaly close to the border of the survey area. There were no other outcrops at the centre of the anomaly Number 2 and at the location of the other anomalies Numbers 1 and 3.

5. Three-dimensional (3D) inversion

The large parts of the inversion methodology and the associated mathematical concepts are described by Camacho *et al*. (2002); the key concepts of which are briefly summarized here. This method seeks to determine the geometry of an indefinite number of anomalous bodies with prescribed (fixed or variable) density contrasts. Positive and negative values of density contrast are accepted. The approach is based on a prismatic partition of the subsurface and attempts to determine the anomalous bodies by means of a "growth" sequence to analyze several model possibilities. Moreover, a regional trend for the gravity data

can be adjusted simultaneously. A number of irregular distributed gravity stations can be considered. To determine the geometry of the anomalous bodies, we decompose the neighboring subsurface volume into a 3D grid of contiguous cells. The adopted basic cell, *j*, *j*=1,..., m is a parallelepiped whose attraction for unit mass density at the survey point *i*, *i*=1….n, can be calculated through Eq. (3). With these basic elements, the anomalous bodies by an expansion or growth process (filling the cells of a 3D grid with the prescribed density contrast, step by step) will be determined.

Suppose that *k*-1 cells have been filled with their density contrast values, the gravity anomaly of this (*k*-1)-th model upon the *i*-th station is:

$$g_i^{(k-1)} = \sum_j a_{i,j} \Delta\rho_j \tag{6}$$

where g_i is the gravity effect, a_{ij} is the non-linear term describing the geometric effect, and $\Delta\rho_j$ is the linear parameter of density.

In an iteration process, the residuals for the gravity stations obtained are:

$$\Delta g_i - (g_i^{k-1} + a_{ij}\Delta\rho_j) f_k - (P_0^k + P_x^k (x_i - x_M) + P_y^k (y_i - y_M) = v_i^k \tag{7}$$

where Δg_i is the observed gravity anomaly, v_i^k represents the residuals and f_k, P_0^k, P_1^k, P_y^k are the unknown values for the scale factor as well as the linear trend for step *k*. The minimization condition used in the method is (Camacho *et al*., 2002):

$$v_k^T Q_D^{-1} v_k + \lambda f_k^2 m_k^T Q_M^{-1} m_k = \min \tag{8}$$

where Q_D is the data covariance matrix, v_k is the vector of residuals for the *k*-th step, m_k represents the density contrasts in the *k*-th model, λ is a positive factor fixed to balance between model fitness and model smoothness and Q_M is an a prior covariance matrix for uncertainties of the model parameters. Camacho *et al*. (1997) suggest to take a model matrix Q_M^{-1} given by a diagonal normalizing matrix of non-null elements that are the same as the diagonal elements of $A^T Q_D^{-1} A$ with matrix *A* of elements A_{ij} from Eq. (1).

The value given by Eq. (8) was chosen as the suitability parameter for the *j*-th cell and its density contrast. After testing each *j*-th cell and its density contrast, the cell and the density contrast that minimized Eq. (8) were selected as the optimum expansion for this *k*-th step.

This inversion method has been developed by Camacho *et al*. (2011) based on the expressed method (Camacho *et al*., 2002).

In new developed algorithm, several novelties are incorporated as follows: 1) a Graphical User Interface (GUI); 2) automatic calculation of λ; 3) optional determination of values for minimum density contrast; 4) an effective handling of outlier data; 5) improved automated data reduction for terrain effects based on anti correlation with topographic data.

Therefore a new code GROWTH2.0 (Camacho *et al*., 2011) has been developed from an earlier one (Camacho *et al*., 2002). It is worth to mention that one of the capabilities of these codes is reserve estimation.

The 3D inversion package presented by Camacho *et al*. (2011) is applied to model the main positive anomalies in two windows (Fig. 5). The method is applied in these two windows and the specifications of the cells are demonstrated in Table 2.

Table 2 - Cell's specifications of 3D inversion.

No. of window	The size of the basic cell (m)	No. of cells	Minimum height of cells (m)	Maximum height of cells (m)
1	6	6695	1753	1840
2	5	2825	1694	1763

The results of the 3D modeling for the selected windows are reflected in Figs. 6 and 7 for windows numbered 1 and 2, respectively.

These figures show the sections passing through the centre of the windows and the horizontal sections of the density contrasts from heights 1810 (Fig. 6a) to 1760 m (Fig. 6c) in the window Number 1 and form heights 1730 (Fig. 7a) to 1710 m (Fig. 7b) in window Number 2 which are provided through GROWTH2.0 code and its GUI.

Inspecting the figures, the horizontal and vertical expansion of the ore-body and the estimated density contrasts can be obtained readily. These results were mostly confirmed by several bore-holes in the survey area. The results of the interpretation process and the 3D inversion are summarized in Table 3.

Table 3 - Results of 3D inversion.

Maximum Density Contrast (kg/m^3)	Maximum height (m)	Minimum height (m)	No.of anomaly
about 850	1730	1710	1
about 416	1750	1810	2
about 416	1750	1810	3

The density contrasts in the two windows were set as the free parameters in the inversion code. The reserve estimations for these windows were 246,000 and 75,000 tons for windows.

Numbers 1 and 2, respectively which were estimated by the inversion algorithm. Therefore, the total reserve estimation was equal to 321,000 tons.

6. Bore-hole results and comparison to 3D inversion

For the confirmation of the inversion results, several bore-holes particularly at the pick of the positive anomalies were drilled in the survey area (Fig. 5). The coordinates and the depths encountering to the ore body of these bore-holes are demonstrated in Table 4.

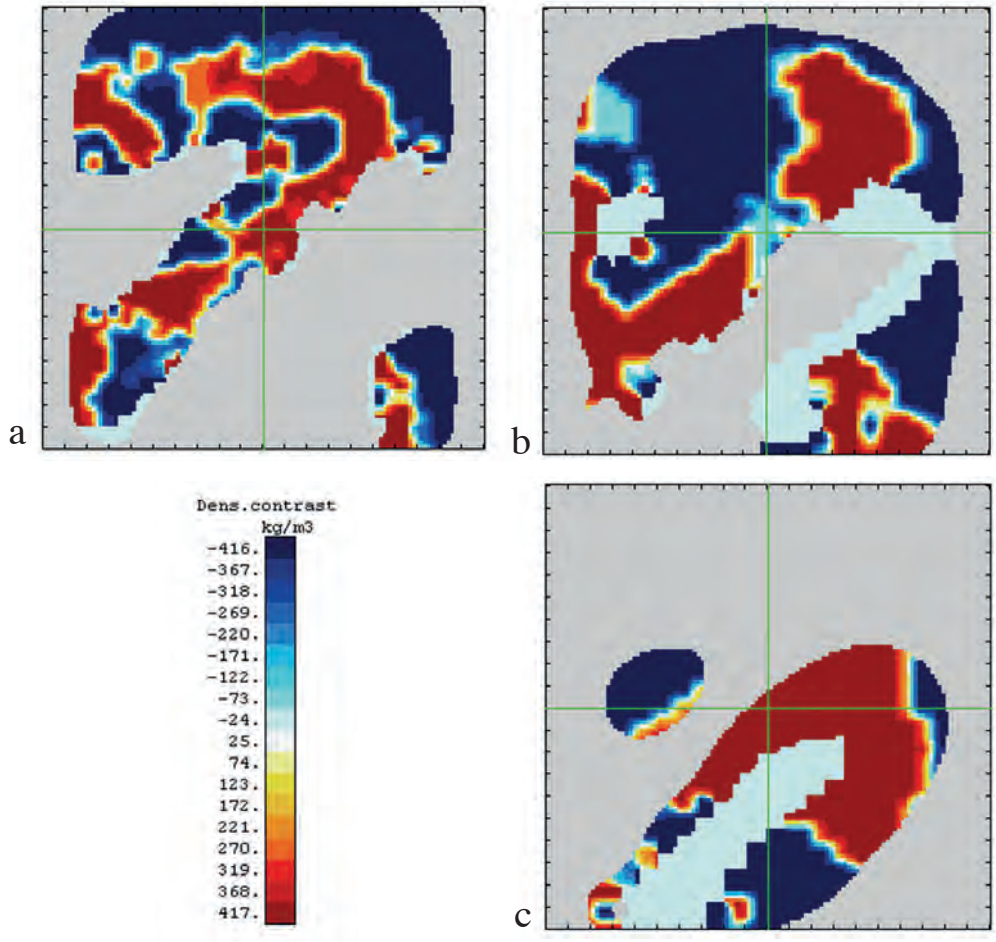

Fig. 6 - The density contrasts in horizontal section of window No. 1 in height 1810 m (a), 1790 m (b) and 1760 m (c).

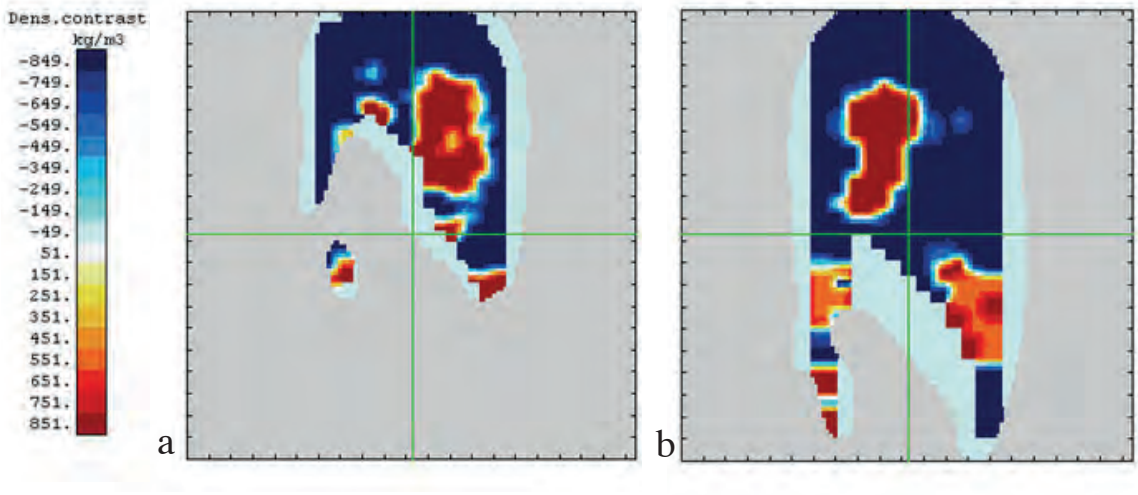

Fig. 7 - The density contrasts in horizontal section of window No. 2 in height 1730 m (a) and 1710 m (b).

Table 4 - Bore-hole results.

No.	X (UTM)	Y (UTM)	Depth of drilling (m)	Depth of Ore body Min.-Max (m)	Number of Anomaly (Fig. 5)
1	704425	4130850	8	2-6	2
2	704448	4130872	10	5-7	2
3	704457	4130884	9	2-9	2
4	704453	4130881	6	3-6	2
5	704369	4130803	6	0	-
6	704392	4130765	10	0	-
7	704461	4130891	14	3-12	2
8	704385	4130823	11	0	-
9	704451	4130877	12	3-12	2
10	704432	4130856	11	4-9	2
11	704412	4130838	8	2-6	2
12	704386	4130826	12	1-4	Between 1 and 2
13	704394	4130826	11	1-4	Between 1 and 2

Table 4 shows that most of the bore-holes are situated in or around the anomaly Number 2 due to its accessibility in mining operations and its closeness to the main outcrop of the ore body. The samples in bore-holes numbered 5, 6 and 8 are mostly formed from hematite which is the main gange contaminating the ore body. Therefore, considering the results of bore-holes numbered 1, 2, 3, 4, 7, 9, 10 and 11, we were able to claim that a huge reserve with no outcrop was detected at the location of the anomaly Number 2. This anomaly was also observable in sections provided by a 3D inversion package from heights 1810 to 1790 m (20 m thickness) in Figs. 6a and 6b. This thickness was partly caused by a manganese ore body particularly in the location of the bore-holes numbered 7 and 9 (Table 4) where they show 12 m as the maximum depth of the ore body. Inspecting Fig. 6 reveals that the positive density contrast at the location of anomaly Number 3 is distinguishable from heights 1810 to 1760 m. Of course, as there is no drilled bore-hole in this area, the cause of this anomaly (either manganese or hematite) is not still confirmed.

Encountering the bore-holes numbered 12 and 13 to ore body was also quite promising for the existence of manganese at the location of anomaly Number 1. On the other hand, the 3D inversion results in window Number 2 that included anomaly Number 1, show the existence of the positive density contrast from heights 1730 to 1710 m (Fig. 7) in the northern part of this

anomaly. Therefore, encountering the ore body especially in the northern part of this anomaly in future bore-holes is very likely.

The estimated density contrasts through the 3D modeling can also be assessed by the bore-hole results. The percent grade of manganese differed from 18 to 60% in the samples obtained from the bore-holes showing an average of about 40%. Considering the density contrast between the ore body (manganese with 4500 kg/m^3 density) and the host rock (andesite with 2500 kg/m^3 density) that is about 2000 kg/m^3 and multiplying the average percent grade (40%) by 2, we have 800 kg/m^3 that is equal to the maximum density contrast obtained through 3D modelling in window Number 2 and for anomaly Number 1. Therefore, we expect an ore body of about 800 kg/m^3 density contrast for anomaly Number 1 that should be investigated by future bore-holes.

It is worth to mention that most samples obtained from bore-holes showed the a percent grade of about 20 and this confirmed the maximum estimated density contrast by the 3D modelling in Window 1 (about 417 kg/m^3).

7. Conclusion

The microgravity method is quite able to detect ore bodies with a sufficient density contrast. The method can also be used to determine the geometrical shape of the source body by the modelling process. Considering the 3D inversion, it gives more accurate and realistic results, especially in the case of the density contrast and depth. Considering the capability of the modelling method, some relatively accurate results can be gained for reserve estimations which are the most important information for mining companies and individuals. Of course, these results should be approved by drilling as it was carried out for the most important anomalies in this case study.

Acknowledgments. The author is thankful to Saeed Salimi Davarzan for collecting the data and other authorities of the Institute of Geophysics, University of Tehran. Special thanks should be given to the Spadana Mining Company for providing geological maps, bore-hole results and financial support. I am also grateful to respected reviewers for their fruitful and instructive comments.

REFERENCES

Ardestani E.V.; 2008: *Modeling the karst zones in a dam site through micro-gravity data*. Explor. Geophys., **39**, 204-209.

Ardestani E.V.; 2010: *Delineating and modeling an underground water conduit by scattered micro-gravity data and electrical resistivity sounding*. Explor. Geophys., **41**, 210-218.

Arzi A.A.; 1975: *Microgravimetry for engineering applications*. Geophys., **23**, 408- 425.

Butler S.J.; 1984: *Microgravimetric and gravity gradient techniques for detection of subsurface cavities*. Geophys., **49**, 1084-1096.

Camacho A.G., Montesinos F.G. and Vieira R.; 1997: *A three-dimensional gravity inversion applied to Sao Miguel Island (Azores)*. J. Geophys. Res., **102**, 7705-7715.

Camacho A.G., Fuensanta G.M. and Viera R.; 2002; *A 3-D gravity inversion tool based on exploration of model possibilities*. Comput. Geosci., **28**, 191-204.

Camacho A.G., Fernandez J. and Gottsmann J.; 2011: *3-D gravity inversion Package GROWTH2.0 and its application to Tenerife Island, Spain*. Comput. Geosci., **37**, 621-633.

Fajklewicz Z.J.; 1976: *Gravity vertical gradient measurements for the detection of small geologic and anthropomorphic forms*. Geophys., **41**, 1016-1030.

Kane M.F.; 1962: *A comprehensive system of terrain corrections using a digital computer*. Geophys., **27**, 455-462.

Nagy D.; 1966: *The gravitational attraction of a right rectangular prism*. Geophys., **31**, 362-371.

Noorizadeh A.; 2010: *Geological report, bore-hole results of Safo manganese mine*. Spadana Mining Company, Esfahan, Iran, 12 pp.

Telford W.M., Geldart L.P., Sheriff R.E. and Keys D.A., 1981: *Applied geophysics*. Cambridge University Press, Cambridge, U.K, 860 pp.

Corresponding author: Vahid E. Ardestani
Institute of Geophysics, University of Tehran, Iran
Kargar Shomali, Tehran, Iran
Phone: +98 21 61118232, fax: +98 21 61118272, e-mail: ebrahimz@ut.ac.ir